Available online at www.sciencedirect.com
ScienceDirect
Progress in Natural Science 19 (2009) 55–63
Progress in Natural Science
www.elsevier.com/locate/pnsc

Quantitative analysis of torrential rainfall associated with typhoon landfall: A case study of typhoon Haitang (2005)

Caijun Yue [a,b,*]

[a] *Shanghai Typhoon Institute, the china Meterological Administration Shanghai 200030, China*
[b] *Laboratory of Typhoon Forecast Technique/China Meterological Administration, Shangai 200030, China*

Received 10 February 2008; received in revised form 18 June 2008; accepted 23 July 2008

Abstract

A quantitative analysis of torrential rainfall associated with typhoon Haitang (2005) is carried out using a modified moist ageostrophic $\boldsymbol{Q}$ vector and data from Weather Research and Forecasting (WRF) model simulation. Four major factors determining the ascending motion associated with torrential rainfall have been studied: large-scale and convective condensational heating, topographic lifting and friction. The results show that the convective condensational heating plays a major role in the torrential rainfall process, and the large-scale condensational heating is secondary before the landfall of typhoon Haitang, and vice versa after the landfall. The topographic lifting affects the formation of rainfall, whereas the topographic friction has important impacts on torrential rainfall after the landfall. The rainfall amounts forced by the topographic friction and lifting have similar horizontal distributions, but the magnitudes of the former are 2–3 times larger than those of the latter. The rainfall amounts forced by topography (lifting and friction) and modified moist ageostrophic $\boldsymbol{Q}$ vector have different horizontal distributions, and the magnitudes of the former are 2–5 times larger than those of the latter. Synthetic analysis shows that the typhoon rainfall may be motivated by modified moist ageostrophic $\boldsymbol{Q}$ vector and enhanced further by the topographic effects.

Keywords: Torrential rainfall; Typhoon landfall; Modified moist ageostrophic $\boldsymbol{Q}$ vector; Topography; Condensational heating; Quantitative analysis

1. Introduction

The landfall of typhoons induces torrential rainfall and causes severe natural disasters, which leads to heavy losses of human lives and local economy. The quantitative precipitation forecast (QPF) of typhoon landfall faces a large challenge [1–4]. Since the torrential rainfall is associated with strong ascending motion, the $\boldsymbol{Q}$ vector that is the forcing of vertical velocity (ω) equation has been paid much attention by meteorological research communities and is an efficient and advanced tool for diagnosing vertical motion [5]. It has been widely used for diagnosis and forecast of various weather systems [6,7] since its introduction by Hoskins et al. [8]. The analysis of $\boldsymbol{Q}$ vector can also be applied to diagnose torrential rainfall associated with the typhoon landfall. Deng and Yang [9] carried out a diagnostic analysis of anomalous intensification of rainfall from typhoon Jeff (8506) with quasi-geostrophic $\boldsymbol{Q}$ vector. Huang et al. [10] also conducted an analysis of torrential rainfall associated with the landfall of typhoon Doug (9405) over northern China and found that the torrential rainfall was intimately related to the convergence of quasi-geostrophic $\boldsymbol{Q}$ vector at 700 hPa. Li et al. [11] calculated frontogenetical function of quasi-geostrophic $\boldsymbol{Q}$ vector of convective development of typhoon Herb (9608) associated with the torrential rainfall over southwestern Hebei. Yao et al. [12–14] studied the same rainfall case with

* Tel.: +86 21 54896098; fax: +86 21 64391966.
E-mail address: yuecaijun2000@163.com

1002-0071/$ - see front matter © 2008 National Natural Science Foundation of China and Chinese Academy of Sciences. Published by Elsevier Limited and Science in China Press. All rights reserved.
doi:10.1016/j.pnsc.2008.07.007

the moist ageostrophic $\boldsymbol{Q}$ vector and showed that the moist ageostrophic $\boldsymbol{Q}$ vector at 800 hPa could be used to examine the evolution of the torrential rainfall. Guo et al. [15] analyzed torrential rainfall in Yunnan Province caused by a westward-propagating low depression system associated with typhoon Imbudo (0307) in 2005, and revealed a correlation between heavy rainfall and the convergence of moist ageostrophic $\boldsymbol{Q}$ vector. Yan and Cai [16] performed a diagnostic analysis of torrential rainfall in typhoon Rananim (0414) with the moist ageostrophic $\boldsymbol{Q}$ vector, and found that the area of negative values of divergence of moist ageostrophic $\boldsymbol{Q}$ vector at 850 hPa is highly correlated with the heavy rainfall area in the next 12 h. Yang et al. [17] studied torrential rainfall over Fujian Province caused by typhoon Aere (0418), and showed that the typhoon rainfall was located over intersection between convergence and divergence of moist ageostrophic $\boldsymbol{Q}$ vector in the lower troposphere. Recently, we [18] modified moist ageostrophic $\boldsymbol{Q}$ vector by including convective condensational heating. Many studies [19–37] have proved that partition of $\boldsymbol{Q}$ vector is a very useful tool for studying weather processes and structures.

In addition to dynamic and thermodynamic effects on rainfall, topography significantly affects rainfall processes [38,39]. Lin et al. [40] showed that the torrential rainfall was mainly caused by topography rather than dynamics. Chiao and Lin [41] carried out numerical simulations to study topographic effects of tropical storm Rachel on rainfall, and found that terrain enhanced the convergence and convective development which intensified rainfall. Duan and Chen [42] revealed that wet condition and topography-induced meso-scale convective system (MCS) led to torrential rainfall in typhoon Fitow (0114). Niu et al. [43] showed that windward could enhance rainfall whereas leeward could suppress rainfall. Recently, Ji et al. [44] from their numerical experiments found that during typhoon Rananim (0414), topography enhanced the rainfall by 40% over eastern Zhejiang Province. Colle [45] showed that the exclusion of terrain could only reduce rainfall amount by 10–30%, indicating a secondary role of terrain in determining rainfall over northeastern US in Hurricane Floyd (1988). Li et al. [46] showed that the rainfall was initially induced by spiral cloud bands inside the typhoon rather than the terrain during the landfall of typhoon Aere (0418). In a previous study [47], the rainfall amount caused by modified moist ageostrophic $\boldsymbol{Q}$ vector and topography was calculated, and the causes of asymmetric distributions of rainfall associated with typhoon Haitang (2005) were analyzed. In this study, modified moist ageostrophic $\boldsymbol{Q}$ vector was partitioned and topographic effects were examined to study the torrential rainfall associated with typhoon Haitang (2005).

2. Typhoon Haitang (2005) and its numerical simulation

Typhoon Haitang (2005) formed over the Pacific Ocean northeast to Guam at 0000 UTC 12 July 2005 and propagated westward while intensifying. It made the landfall over Yilan, Taiwan Island at 0650 UTC 18 July and crossed Taiwan Strait, then made another landfall over Huangqi, Lianjiang, Fujian Province at 0910 UTC 19 July. Afterward, it moved northwestward within Fujian Province, and finally entered Jiangxi Province through northern Fujian Province. Fig. 1 shows cumulative rainfall amounts of $\geqslant 50$ mm over the period of 24 h in 27 stations located in Fujian and Zhejiang provinces (26.5°N–30°N, 119°E–122°E) during the landfall of typhoon Haitang (2005) (0000 UTC 19 July–0000 UTC 20 July 2005). Among them, rainfall amounts reached 100 mm in a 24-h period in 18 stations, 200 mm in 10 stations and 250 mm in 9 stations. The maximum rainfall amounts of 411 and 384 mm over the period of 24 h occurred over 28.11°N, 120.95°E and 27.85°N, 121.18°E, respectively.

Weather Research and Forecasting (WRF) model is a new meso-scale model developed by US meteorological communities. It has been shown that WRF model is capable of simulating typhoon Haitang (2005) during the landfall with the location error of 20 km [47]. With a linear interpolation technique, the outputs from numerical simulations were matched to the observational stations, which showed rainfall amounts of 50 mm and more in 24 stations, 100 mm in 17 stations, 200 mm in 9 stations, and 250 mm in 3 stations over the period of 24 h. The maximum rainfall amounts of 402 and 353 mm over the period of 24 h occurred over 28.38°N, 121.35°E and 28.08°N, 121.26°E, respectively. This demonstrates that the model simulates location and intensity of rainfall well. Thus, the areas with the rainfall amount of $\geqslant 50$ mm (shaded area in Fig. 1) were analyzed in this study, and the data over this area were averaged. Results showed that the rainfall amount increased gradually from 0000 UTC to 0400 UTC 19 July before the landfall of typhoon Haitang (2005), and decreased from 0400 UTC to 0700 UTC 19 July when the typhoon made the landfall, then increased and reached its maximum of 8.8 mm h^{-1} around 1500 UTC 19 July 2005, and finally dissipated quickly after.

3. Calculation of condensational heating and modified moist ageostrophic $\boldsymbol{Q}$ vector

Total condensation heating associated with typhoon rainfall (H) consists of large-scale (Hs) and convective (Hc) condensational heating. Hs can be calculated based on Ding [48] and Yue et al. [18], whereas Hc can be calculated based on Kuo [49,50] and Yue et al. [18]. The calculations obtained in this study showed that the evolution of total condensational heating was intimately associated with that of hourly cumulative rainfall amount (Figs. 2 and 3). Convective condensational heating mainly accounted for total condensational heating from 0100 UTC to 0800 UTC 19 July, and large-scale condensational heating became larger than convective heating from 0900 UTC to 1900 UTC 19 July, and large-scale and convective condensational heating became equally important after 2000 UTC

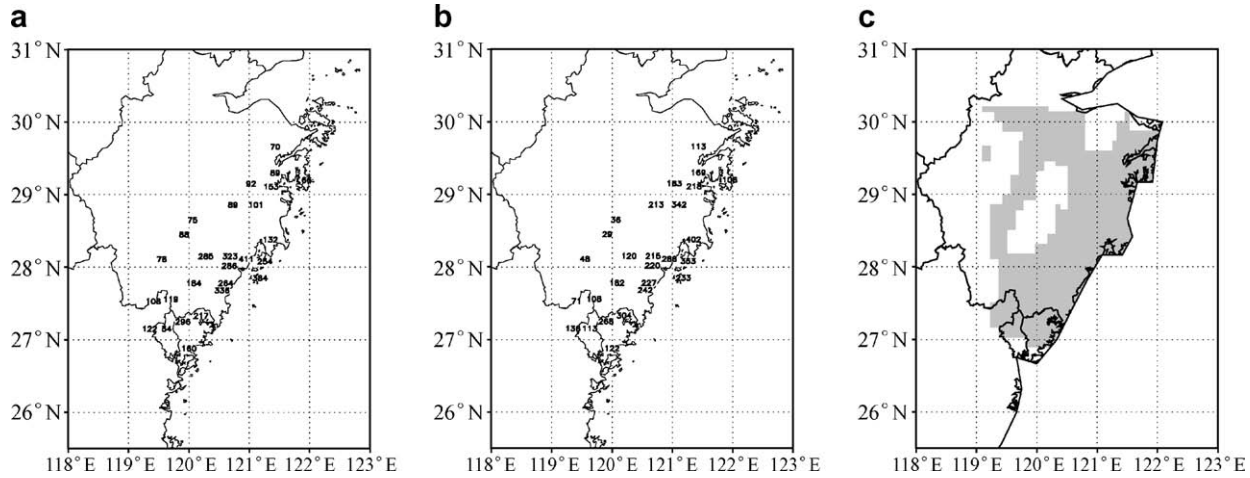

Fig. 1. Cumulative rainfall amount (mm) from 0000 UTC 19 July to 0000 UTC 20 July 2005 (a) and numerical simulations (b and c). The areas with more than 50 mm rain filed in a 24 h period are shaded.

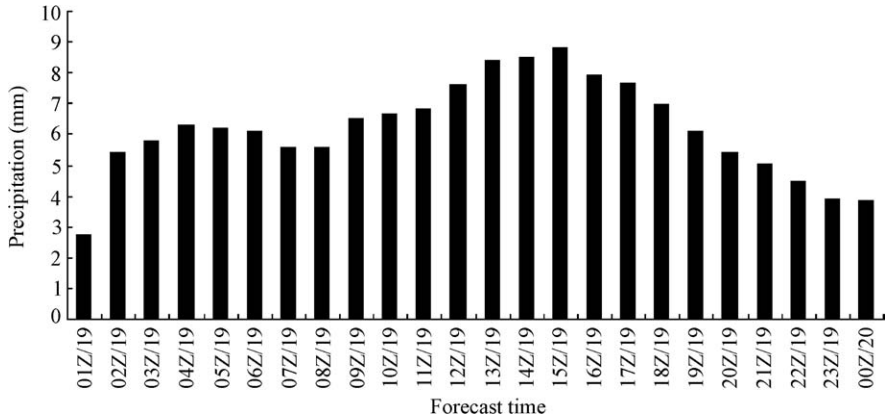

Fig. 2. Area-averaged hourly cumulative rainfall amount (mm) from 0000 UTC 19 July to 0000 UTC 20 July 2005.

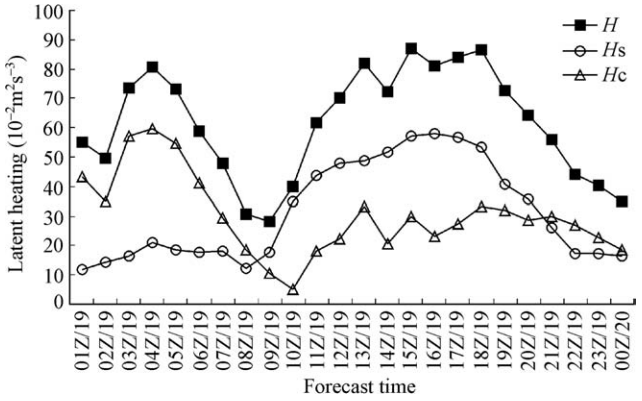

Fig. 3. Time series of area-averaged total (H), large-scale (Hs), and convective condensational (Hc) heating rates (10^{-2} m^2 s^{-3}) in air column (1000–100 hPa).

19 July 2005. The magnitude of Hc was 2–5 times larger than that of Hs before the landfall of the typhoon. The magnitude of Hs was about twice larger than that of Hc in 11 h after the landfall. The comparison between convective condensational heating and hourly cumulative rainfall amount indicated that the maximum convective condensational heating appeared before the landfall whereas maximum rainfall amount occurred after the landfall.

$\boldsymbol{Q}$ vector represents contributions from dynamic and thermodynamic processes, and a modified moist ageostrophic $\boldsymbol{Q}$ vector ($\boldsymbol{Q}^*$) contains large-scale and convective condensational heating. Thus, $\boldsymbol{Q}^*$ vector has been analyzed.

Following Ref. [18], $\boldsymbol{Q}^*$ vector in p-coordinate can be expressed as

$$Q_x^* = \frac{1}{2}\left[f\left(\frac{\partial v}{\partial p}\frac{\partial u}{\partial x} - \frac{\partial u}{\partial p}\frac{\partial v}{\partial x}\right) - h\frac{\partial V}{\partial x}\cdot\nabla\theta + \frac{R}{C_p p}\frac{\partial}{\partial x}(H\mathrm{s} + H\mathrm{c})\right] \tag{1}$$

$$Q_y^* = \frac{1}{2}\left[f\left(\frac{\partial v}{\partial p}\frac{\partial u}{\partial y} - \frac{\partial u}{\partial p}\frac{\partial v}{\partial y}\right) - h\frac{\partial V}{\partial y}\cdot\nabla\theta + \frac{R}{C_p p}\frac{\partial}{\partial y}(H\mathrm{s} + H\mathrm{c})\right] \tag{2}$$

where $h = \frac{R}{p}\left(\frac{p}{1000}\right)^{R/C_P}$; $\boldsymbol{Q}_x^*$, $\boldsymbol{Q}_x^*$ are zonal and meridional components of $\boldsymbol{Q}^*$ vector, respectively; the others are conventional physical variables. The ageostrophic ω equation can be written by

$$\nabla^2(\sigma\omega) + f^2\frac{\partial^2\omega}{\partial p^2} = -2\nabla\cdot \mathrm{Q}^* \tag{3}$$

If diabatic heating is excluded, the modified moist $\boldsymbol{Q}$ vector becomes dry $\boldsymbol{Q}$ vector [51]. Thus, the modified moist ageostrophic $\boldsymbol{Q}$ vector contains contributions from dry ageostrophic $\boldsymbol{Q}$ vector, and large-scale and convective condensational heating. Unlike reported in [37], dry ageostrophic $\boldsymbol{Q}$ vector ($\boldsymbol{Q}^{\mathrm{D}}$) is partitioned in natural coordinate (Fig. 4) into two components: $\boldsymbol{Q}_s^{\mathrm{D}}$ and $\boldsymbol{Q}_n^{\mathrm{D}}$. $\boldsymbol{Q}_s^{\mathrm{D}}$ is along the isotherm line or along the direction of isotherm wind, which is quasi-geostrophic. $\boldsymbol{Q}_n^{\mathrm{D}}$ is perpendicular to the isotherm line, which is ageostrophic [19–25,27–31,33–35,37]. Furthermore, moist ageostrophic $\boldsymbol{Q}$ vector ($\boldsymbol{Q}^*$) can be partitioned into $\boldsymbol{Q}_s^*$ and $\boldsymbol{Q}_n^*$. $\boldsymbol{Q}_s^*$ includes $\boldsymbol{Q}_s^{\mathrm{D}}$ and Hs whereas $\boldsymbol{Q}_n^*$ includes $\boldsymbol{Q}_n^{\mathrm{D}}$ and Hc.

In Fig. 4, $\boldsymbol{n}$ is a unit vector along $\nabla\theta$, and $\boldsymbol{n} = \frac{\nabla\theta}{|\nabla\theta|}$. When $\boldsymbol{n}$ rotates 90° counterclockwise to obtain unit vector $\boldsymbol{s}$, $\boldsymbol{s} = \boldsymbol{k}\times\boldsymbol{n}$, $\boldsymbol{Q}_n^{\mathrm{D}} = \left(\frac{\boldsymbol{Q}^{\mathrm{D}}\cdot\nabla\theta}{|\nabla\theta|}\right)\boldsymbol{n}$, $\boldsymbol{Q}_s^{D} = \frac{\boldsymbol{Q}^{\mathrm{D}}\cdot(\boldsymbol{k}\times\nabla\theta)}{|\nabla\theta|}\left[\frac{(\boldsymbol{Q}\times\nabla\theta)}{|\nabla\theta|}\right]$. For convenience, $\boldsymbol{Q}^* = \boldsymbol{Q}_T^*$. The vertical velocity and rainfall amount forced by $\boldsymbol{Q}_T^*$, $\boldsymbol{Q}_s^*$, and $\boldsymbol{Q}_n^*$ are calculated, respectively, as previously described [47].

The ascending motion forced by $\boldsymbol{Q}^*$ vector and hourly cumulative rainfall amount were found to be highly correlated (Figs. 2 and 5). Hourly cumulative rainfall amount increased as the ascending motion strengthened before 0400 UTC 19 July 2005. Then, hourly cumulative rainfall amount reached its minimum when vertical motion between 700 and 500 hPa changed from weak ascending motion to descending motion ($\sim$0.05 Pa s^{-1}) during the landfall. The rainfall amount reached its maximum around 1500 UTC 19 July while the ascending motion showed its maximum of -0.35 Pa s^{-1} at 650 hPa at 1600 UTC 19 July. It should be noticed that ascending motion does not dominate throughout the troposphere during its life span. Instead, descending motion may appear in the mid-troposphere during the landfall.

We observed that the evolution and vertical structure of ω_n^* (Fig. 5) was similar to that of ω^* (Fig. 5), indicating that ω_n^* plays a primary role in determining ω^* while ω_s^* is secondary, which also reveals that meso-scale component serves as a main factor in forcing ascending motion whereas large-scale component plays a diminishing role. Horizontal distributions of 24-h cumulative rainfall amount forced by $\boldsymbol{Q}_T^*$, $\boldsymbol{Q}_s^*$, and $\boldsymbol{Q}_n^*$ (Fig. 6) show that the rainfall amount forced by $\boldsymbol{Q}_s^*$ is much weaker than that forced by $\boldsymbol{Q}_n^*$ so that horizontal distribution of rainfall amount forced by $\boldsymbol{Q}_T^*$ is determined by that forced by $\boldsymbol{Q}_n^*$.

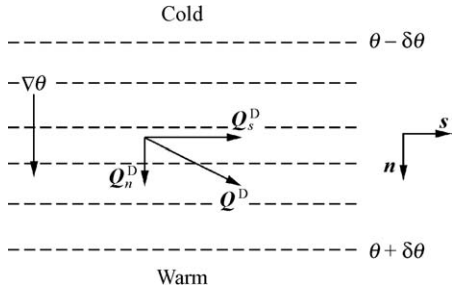

Fig. 4. Partition of $\boldsymbol{Q}^{\mathrm{D}}$.

4. Effects of topography

As aforementioned, effects of topography (WTF) on the typhoon rainfall are from lifting and friction. Thus, vertical velocity induced by topography is the sum of lifting-induced (WT) and friction-induced (WF) vertical velocity, which can be, respectively, calculated based on Ref. [47]. Correspondingly, the rainfall due to topography is comprised of the rainfall due to lifting and friction. Fig. 7 shows the topography-forced ascending motion during the landfall of typhoon Haitang (2005). The ascending motion (~-0.5 Pa s^{-1}) did not change much before the landfall, and increased to -2 Pa s^{-1} around 1800 UTC 19 July 2005 after the landfall. The evolution of the ascending motion forced by topography was similar to that of hourly cumulative rainfall amount (Fig. 2) only after the landfall. The lifting-induced ascending motion kept its magnitude (~-1 Pa s^{-1}) during the landfall, while the friction-induced vertical motion showed a significant evolution. The friction-induced descending motion ($\sim$0.5 Pa s^{-1}) appeared before the landfall whereas the friction-induced vertical

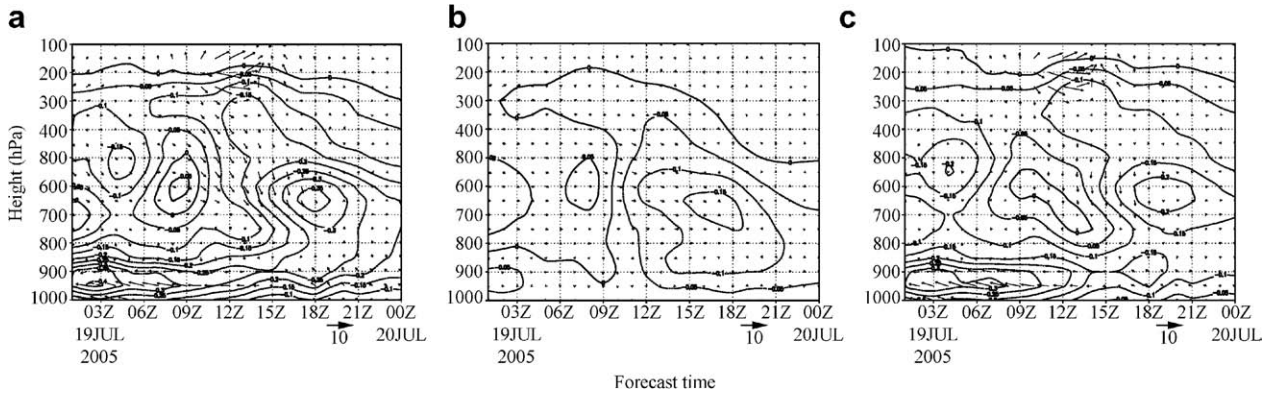

Fig. 5. Area averaged ω^* (a), ω_s^* (b), and ω_n^* (c) (contour: Pa s^{-1}), and corresponding $\boldsymbol{Q}^*$ vector (10^{-10} m hPa^{-1} s^{-3}).

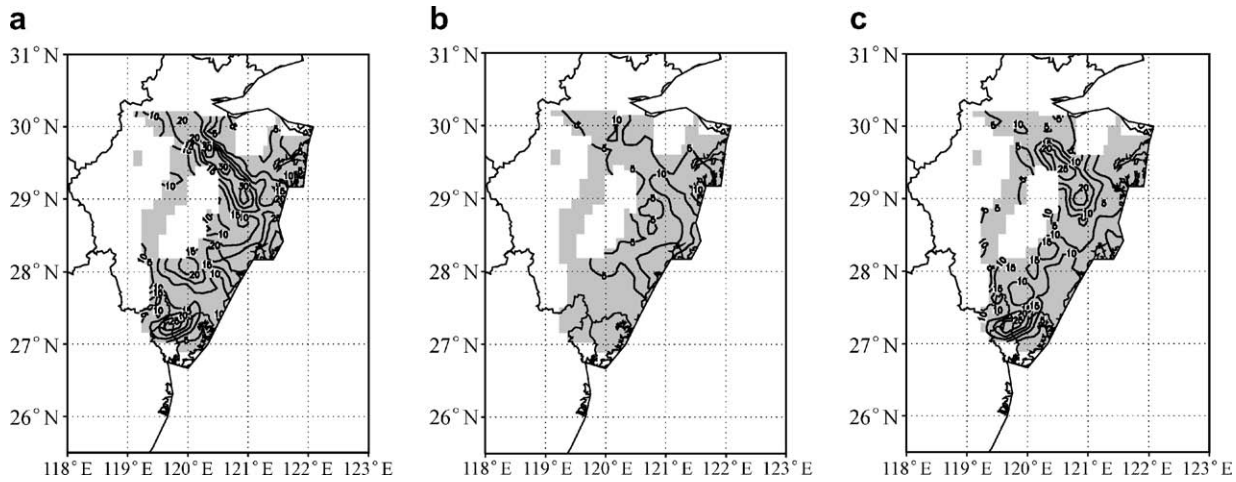

Fig. 6. Cumulative rainfall amounts (mm) forced by $2\nabla \cdot \boldsymbol{Q}_T^*$ (a), $2\nabla \cdot \boldsymbol{Q}_s^*$ (b), and $2\nabla \cdot \boldsymbol{Q}_n^*$ (c). Areas with the rainfall amount of $\geqslant 50$ mm in 24 h are shaded.

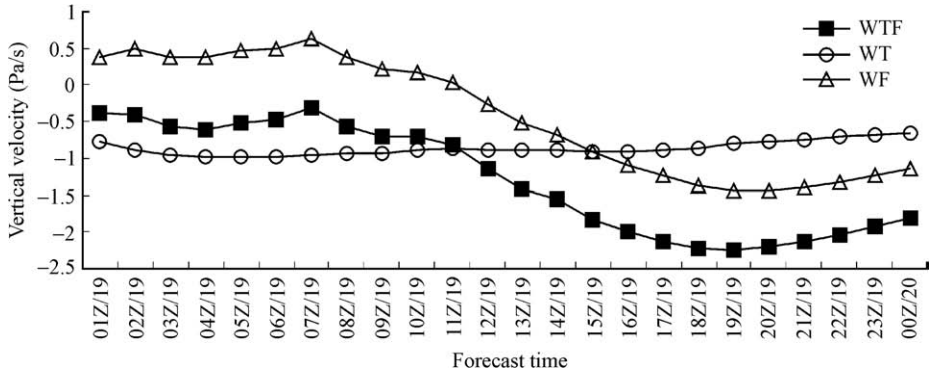

Fig. 7. Area-averaged lifting-induced (WT), and friction-induced (WF) vertical motions and their sum (WTF). The units are Pa s^{-1}.

motion became an ascending motion after the landfall and increased its intensity with time. The magnitudes of friction-induced ascending motion were larger than those of lifting-induced ascending motion after 1200 UTC 19 July 2005. The horizontal distributions of 24-h cumulative rainfall amounts forced by topographic lifting and topographic friction were similar, but the maximum friction-induced rainfall amount could be 2–3 times larger than the maximum lifting-induced rainfall amount (Fig. 8). Therefore, topographic friction has made more contribution to 24-h cumulative rainfall amount than topographic lifting made.

5. Discussion

5.1. Roles of modified moist ageostrophic $\boldsymbol{Q}$ *vector and topographic forcing in rainfall*

Both modified moist ageostrophic $\boldsymbol{Q}$ vector and topographic forcing show impacts on the ascending motion and rainfall of typhoon Haitang (2005). To examine their relative importance, the 24-h cumulative rainfall amounts produced by both topographic forcing (Fig. 9) and the modified moist ageostrophic $\boldsymbol{Q}$ vector (Fig. 6) are calculated. The differences in the rainfall amount between the modified moist ageostrophic $\boldsymbol{Q}$ vector and topographic forcing show that the rainfall amount forced by topography is larger than that forced by modified moist ageostrophic $\boldsymbol{Q}$ vector and that the centers of rainfall amount induced by topography are located in the coastal areas of Zhejiang Province whereas those forced by the modified moist ageostrophic $\boldsymbol{Q}$ vector are located in central Zhejiang. The area-averaged hourly cumulative rainfall amounts forced by the modified moist ageostrophic $\boldsymbol{Q}$ vector and topographic forcing (Fig. 10) reveal that the latter is 2–5 times larger than the former. Relatively, the topographic contributions to the rainfall of typhoon Haitang (2005) are more than those from the modified moist ageostrophic $\boldsymbol{Q}$ vector.

Although the rainfall amount forced by topography is larger than that forced by the modified moist ageostrophic $\boldsymbol{Q}$ vector (Fig. 10), topography-forced vertical velocity does not show a strong variation (Fig. 7), while the simulated hourly cumulative rainfall amount displays a significant variation (Fig. 2) before the landfall. During this period,

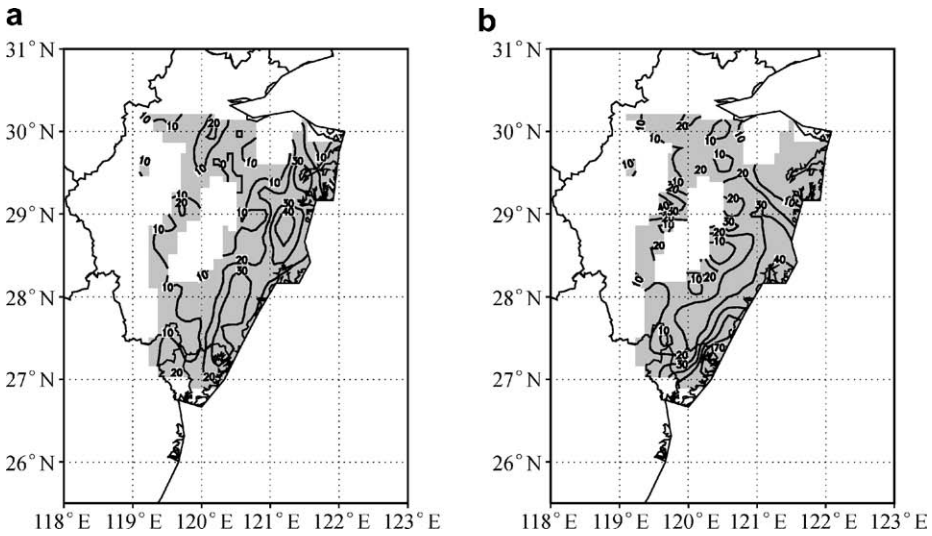

Fig. 8. Cumulative rainfall amounts (mm) forced by topographic lifting (a) and topographic friction (b). Areas with the rainfall amount of $\geqslant 50$ mm in 24 h are shaded.

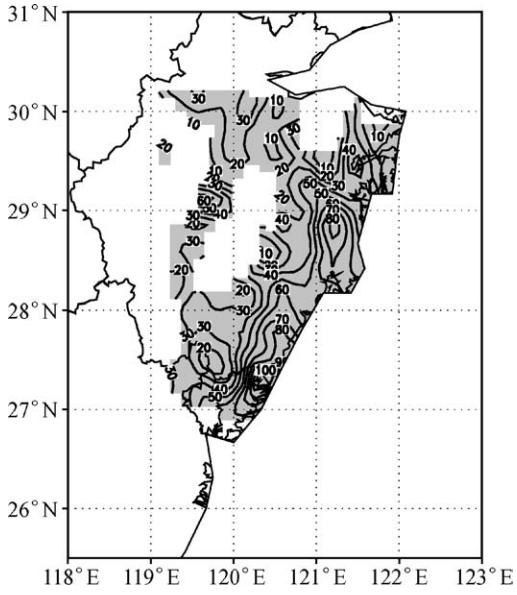

Fig. 9. Cumulative rainfall amounts (mm) produced by both topographic lifting and topographic friction. Areas with the rainfall amount of $\geqslant 50$ mm in 24 h are shaded.

the vertical velocity forced by the modified moist ageostrophic $\boldsymbol{Q}$ vector exhibits a strong variation (Fig. 5), which is similar to the variation of rainfall amount (Fig. 2). Specifically, the strong ascending motion leads to large rainfall, and the rainfall becomes weak during the landfall, which is caused by the descending motion in the mid and lower troposphere (500–700 hPa). After the landfall, effects of topography on vertical motion are similar to the effects of $\boldsymbol{Q}^*$ vector. What roles do they play in torrential rainfall during the landfall? It is well known that the environmental conditions surrounding the typhoon change quite rapidly while topography remains unchanged. Topography affects the rainfall through its interaction with typhoon. Combining the previous analytical results, we think that the modified moist ageostrophic $\boldsymbol{Q}$ vector that represents physical processes may be a factor triggering the formation of torrential rainfall of typhoon Haitang (2005) whereas topography may enhance the rainfall through local nonlinear processes. Topographical effects on torrential rainfall may play a dominant role.

5.2. Comparison of the rainfall diagnosis with the simulated results

To examine the ability of diagnostic tool for producing rainfall amount, the horizontal distribution of 24-h cumulative rainfall amount and the area-averaged hourly cumulative rainfall amount forced by the modified moist ageostrophic $\boldsymbol{Q}$ vector and topographic forcing are compared with those simulated by the WRF model. The horizontal distributions of 24-h cumulative rainfall amounts simulated by the model and calculated by the modified moist ageostrophic $\boldsymbol{Q}$ vector and topographic forcing are similar (Fig. 11), but the magnitudes of rainfall simulated by the model are significantly larger than those calculated by the modified moist ageostrophic $\boldsymbol{Q}$ vector and topographic forcing (Fig. 12).

As shown in Fig. 12, the rainfall amount forced by the modified moist ageostrophic $\boldsymbol{Q}$ vector and topographic forcing is significantly smaller than that simulated by the model, which is consistent with the results from the previous studies [52–54]. As aforementioned in Section 2, the simulated rainfall amount is similar to the observed rainfall amount (Fig. 1). Thus, diagnostic analysis cannot depict simulated rainfall completely. The reasons may include: (1) cloud microphysical processes intimately associated with precipitation are not included in the diagnostic analysis. (2) Although the modified moist ageostrophic $\boldsymbol{Q}$ vector contains information of atmospheric dynamics and ther-

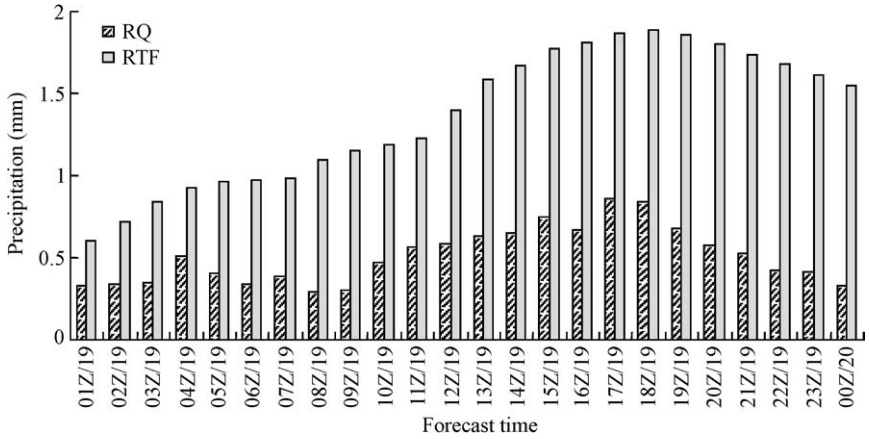

Fig. 10. Area-averaged hourly cumulative rainfall amounts (mm) forced by the modified moist ageostrophic $\boldsymbol{Q}$ vector (RQ) and topographic forcing (RTF).

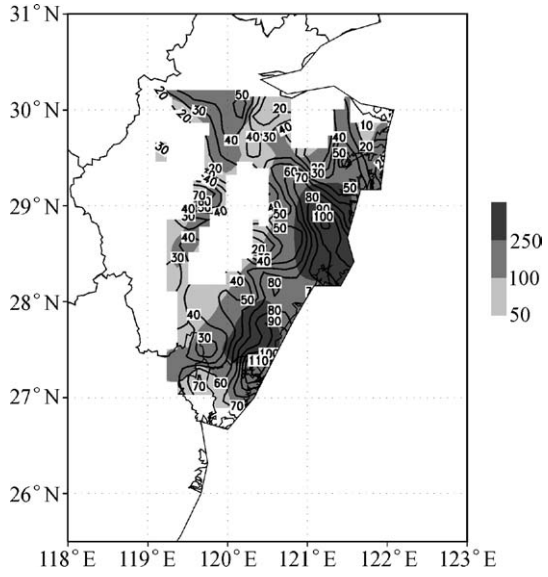

Fig. 11. Cumulative rainfall amounts (mm) simulated by the model (background) and calculated by the modified moist ageostrophic $\boldsymbol{Q}$ vector and topographic forcing (contour) from 0000 UTC 19 July to 0000 UTC 20 July 2005.

modynamics, some important processes such as evaporation are not included and some assumptions are used in derivation of the vector. (3) Although the amounts of rainfall forced by topography are much larger than those forced by $\boldsymbol{Q}^*$ vector (Fig. 10) and topography has significant impacts on torrential rainfall and its horizontal distributions (Figs. 9 and 11), only the linear effects of topography on rainfall are counted in this quantitative diagnostic analysis. The nonlinear interaction between topography and local atmosphere and its effects on rainfall development remain unknown, and are not included in the calculations here, as indicated by Lin et al. [55] that the measurements of winds at certain locations partially provide information of interaction between topography and weather system. (4) Topography used in this study may be much smoother than the real topography and atmospheric stability parameter has been averaged in the calculation, which may underestimate the ascending motion. (5) Rainfall rate is assumed to be a constant when the rainfall amount is calculated, which may lead to underestimation of rainfall amount.

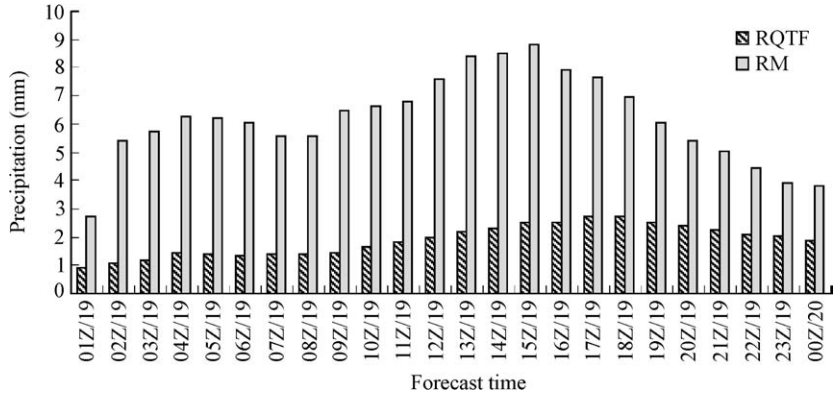

Fig. 12. Area-averaged hourly cumulative rainfall amounts (mm) simulated by the model (RM) and calculated by the modified moist ageostrophic $\boldsymbol{Q}$ vector and topographic forcing (RQTF).

6. Conclusions

A quantitative analysis of torrential rainfall associated with typhoon Haitang (2005) is carried out using a modified moist ageostrophic $\boldsymbol{Q}$ vector and data from Weather Research and Forecasting (WRF) model simulation. The results include:

1. WRF can simulate the rainfall of typhoon Haitang (2005) well, including the magnitudes and locations of torrential rainfall, and a decreasing tendency of rainfall onward from the coastal areas.
2. The condensational heating is highly correlated with the rainfall. The convective condensational heating is dominant before the landfall due to the fact that the convective condensational heating rate is 2–5 times larger than the large-scale condensational heating rate. After the landfall, the large-scale condensational heating rate is about twice larger than the convective condensational heating rate. The large-scale and convective condensational heatings are equally important during the landfall. The maximum convective condensational heating occurs before the landfall whereas the maximum large-scale condensational heating appears after the landfall.
3. The diagnostic analysis of the modified moist ageostrophic $\boldsymbol{Q}$ vector shows that the descending motion could appear in the mid-troposphere during the landfall, which reduces the rainfall. The ascending motion is intimately associated with the rainfall. Meso-scale forcing plays a more important role in determining the ascending motion associated with the torrential rainfall in such a way that large-scale forcing role is secondary.
4. The topography-induced vertical motion has little change before the landfall, and shows evolution after the landfall. The topographic lifting always produces an ascending motion. The topographic friction generates the descending motion before the landfall and yields the ascending motion with intensity stronger than that of the lifting-induced ascending motion after the landfall.
5. The rainfall amount forced by topographic friction is 2–3 times larger than that forced by topographic lifting. The topography-forced rainfall amount is 2–5 times larger than the rainfall amount forced by the modified moist ageostrophic $\boldsymbol{Q}$ vector.
6. The rainfall may be triggered by the forcing from the modified moist ageostrophic $\boldsymbol{Q}$ vector and enhanced further by the topographic effects.

It should be noticed that we referred the rainfall of $\geqslant 50$ mm in the period of 24 h as the torrential rainfall in this study. In our future work, the rainfall at the levels of 50–100 mm, 100–250 mm, and >250 mm in the period of 24 h and the different physical processes responsible for these rainfalls will be explored.

Acknowledgments

This work was supported by the National Natural Science Foundation of China (Grant Nos. 40875025, 40405009, 40075009, and 40205008), Jiangsu Key Laboratory of Meteorological Disaster Funding of China (Grant No. KJS0602), and Shanghai Natural Science Foundation of China (08ZR1422900).

References

[1] Marks FD, Shay LK. Landfalling tropical cyclones: forecast problems and associated research opportunities. Bull Am Meteorol Soc 1998;79(2):305–23.
[2] Elsberry RL, Marks FD. The hurricane landfall workshop summary. Bull Am Meteorol Soc 1999;80(4):683–5.
[3] Elsberry RL. Predicting hurricane landfall precipitation: optimistic and pessimistic views from the symposium on precipitation extremes. Bull Am Meteorol Soc 2002;83(9):1333–9.
[4] Chen LS, Luo ZX, Li Y. Research advances on tropical cyclone landfall process. Acta Meteorol Sin 2004;62(5):541–9, [in Chinese].
[5] Dunn LB. Evaluation of vertical motion: past, present, and future. Wea Forecasting 1991;6(1):65–73.
[6] Yue CJ. The advances on the $\boldsymbol{Q}$ vector and its application to synoptic diagnosis. Meteorol Mon 1999;25(11):3–8, [in Chinese].
[7] Yue CJ, Shou YX, Yao XP, et al. Application and research on $\boldsymbol{Q}$-vector analytic method in China. Plateau Meteorol 2005;24(3):450–5, [in Chinese].
[8] Hoskins BJ, Dagbici I, Darics HC. A new look at the ω-equation. Q J R Meteorol Soc 1978;104(439):31–8.
[9] Deng ZY, Yang MC. The diagnosis of the sudden heavy rain amplification for typhoon 8506. Atmos Sci Res Appl 1997;12(1):23–30, [in Chinese].
[10] Huang WG, Deng BS, Xiong TN. A case study of typhoon torrential rain. Q J Appl Meteorol 1997;8(2):247–51, [in Chinese].
[11] Li ZN, Zheng XJ, Zhao YM, et al. The mesoscale torrential rain cloud cluster from the low pressure periphery area of the typhoon No. 9608. J Trop Meteorol 2000;16(4):316–26, [in Chinese].
[12] Yao XP, Yu YB. Non-geostrophic wet $\boldsymbol{Q}$-vector analysis and its application to typhoon torrential rain. Acta Meteorol Sin 2000;58(4):436–46, [in Chinese].
[13] Yao XP, Yu YB. Perfect $\boldsymbol{Q}$-vector and its diagnoses. Plateau Meteorol 2001;20(2):208–13, [in Chinese].
[14] Yao XP, Yu YB, Shou SW. Diagnostic analyses and application of the moist ageostrophic $\boldsymbol{Q}$ vector. Adv Atmos Sci 2004;21(1):96–102.
[15] Guo RF, Lu YB, Li Y, et al. Analyses of a Yunnan rainstorm process influenced by the "Imbudo" typhoon. Plateau Meteorol 2005;24(5):784–91, [in Chinese].
[16] Yan QD, Cai QB. Application of ageostrophic wet $\boldsymbol{Q}$-vector analysis in torrential rain of typhoon "Rananim". J Trop Meteorol 2006;22(5):505–9, [in Chinese].
[17] Yang YH, Shen XY, Lin LW, et al. Diagnostic analysis and numerical simulation of typhoon Aere rainstorm. Meteorol Mon 2006;32(7):81–7, [in Chinese].
[18] Yue CJ, Shou YX, Shou SW, et al. The improvement and perfection of $\boldsymbol{Q}$ vector. J Trop Meteorol 2003;19(3):308–16, [in Chinese].
[19] Keyser D, Reeder MJ, Reed RJ. A generalization of Petterssen's frontogenesis function and its relation to the forcing of vertical motion. Mon Wea Rev 1988;116(3):762–80.
[20] Keyser D, Schmidt BD, Duffy DG. Quasi-geostrophic vertical motions diagnosed from along- and cross-isentrope components of the $\boldsymbol{Q}$ vector. Mon Wea Rev 1992;20(5):731–41.
[21] Davies-Jones R. The frontogenetical forcing of secondary circulations. Part I: the duality and generalization of the $\boldsymbol{Q}$ vector. J Atmos Sci 1991;48(4):497–509.

[22] Kurz M. Synoptic diagnosis of frontogenetic and cyclogenetic processes. Meteorol Atmos Phys 1992;48(1):77–91.
[23] Barnes SL, Colman BR. Quasigeostrophic diagnosis of cyclogenesis associated with a cut off extratropical cyclone – the Christmas 1987 storm. Mon Wea Rev 1993;121(6):1613–34.
[24] Barnes SL, Colman BR. Diagnosing an operational numerical model using ***Q***-vector and potential vorticity concepts. Wea Forecasting 1994;9(1):85–102.
[25] Schar C, Wernli H. Structure and evolution of an isolated semi-geostrophic cyclone. Q J R Meteorol Soc 1993;119(509):57–90.
[26] Jusem JC, Atlas R. Diagnostic evaluation of vertical motion forcing mechanism by using ***Q***-vector partitioning. Mon Wea Rev 1998;126(8):2166–84.
[27] Martin JE. Quasi-geostrophic forcing of ascent in the occluded sector of cyclones and the trowal airstream. Mon Wea Rev 1999;127(1):70–88.
[28] Martin JE. The separate roles of geostrophic vorticity and deformation in the midlatitude occlusion process. Mon Wea Rev 1999;127(10):2404–18.
[29] Martin JE. The role of shearwise and transverse quasigeostrophic vertical motions in the midlatitude cyclone life cycle. Mon Wea Rev 2006;134(4):1174–93.
[30] Martin JE. Lower-tropospheric height tendencies associated with the shearwise and transverse components of quasigeostrophic vertical motion. Mon Wea Rev 2007;135(7):2803–9.
[31] Morgan MC. Using piecewise potential vorticity inversion to diagnose frontogenesis. Part I: a partitioning of the ***Q*** vector applied to diagnosing surface frontogenesis and vertical motion. Mon Wea Rev 1999;127(12):2796–821.
[32] Donnadille J, Cammas J-P, Mascart P, et al. FASTEX IOP 18: a very deep tropopause fold. II: quasi-geostrophic omega diagnoses. Q J R Meteorol Soc 2001;127(577):2269–86.
[33] Yue CJ, Shou SW, Lin KP, et al. Diagnosis of the heavy rain near a Meiyu front using the wet ***Q*** vector partitioning method. Adv Atmos Sci 2003;20(1):37–44.
[34] Pyle ME, Keyser D, Bosart LF. A diagnostic study of jet streaks: kinematic signatures and relationship to coherent tropopause disturbances. Mon Wea Rev 2004;132(1):297–319.
[35] Thomas BC, Martin JE. A synoptic climatology and composite analysis of the Alberta Clipper. Wea Forecasting 2007;22(2):315–33.
[36] Yue CJ. The ***Q*** vector analysis of the heavy rainfall from Meiyu front cyclone: a case study. Acta Meteorol Sin 2008;66(1):35–49, [in Chinese].
[37] Yue CJ, Dong MY, Shou SW, et al. Improved wet ***Q*** vector's analytical method and the mechanism of Meiyu front rainstorm genesis. Plateau Meteorol 2007;26(1):165–75, [in Chinese].
[38] Tuleya RE, Kurihara Y. A numerical simulation of the landfall of tropical cyclones. J Atmos Sci 1978;35(2):242–57.
[39] Bender MA, Tuleya RE, Kurihara Y. A numerical study of the effect of a mountain range on a landfalling tropical cyclone. Mon Wea Rev 1985;113(4):567–82.
[40] Lin YL, Ensley DB, Chiao S. Orographic influences on rainfall and track deflection associated with the passage of a tropical cyclone. Mon Wea Rev 2002;130(12):2929–50.
[41] Chiao S, Lin YL. Numerical modeling of an orographically enhanced precipitation event associated with tropical storm Rachel over Taiwan. Wea Forecasting 2003;18(2):325–44.
[42] Duan L, Chen LS. Diagnostic analysis and numerical study of torrential rain associated with the tropical storm Fitow (0114). Chin J Atmos Sci 2005;29(3):343–53, [in Chinese].
[43] Niu XX, Du HW, Liu JY. The numerical simulation of rainfall and precipitation mechanism associated with typhoons Sinlaku (0216). Acta Meteorol Sin 2005;63(1):57–68, [in Chinese].
[44] Ji CX, Xue GY, Zhao F, et al. The numerical simulation of orographic effect on the rain and structure of typhoon Rananim during landfall. Chin J Atmos Sci 2007;31(2):233–44, [in Chinese].
[45] Colle BA. Numerical simulations of the extratropical transition of Floyd (1999): structural evolution and responsible mechanisms for the heavy rainfall over the Northeast United States. Mon Wea Rev 2003;131(12):2905–26.
[46] Li YY, Huang W, Zhao JZ. Roles of mesoscale terrain and latent release in typhoon precipitation: a numerical case study. Adv Atmos Sci 2007;24(1):35–43.
[47] Yue CJ. Quantitative study on asymmetric characteristic genesis of precipitation associated with typhoon Haitang. Chin J Atmos Sci 2009;33(1):51–70, [in Chinese].
[48] Ding YH. Diagnostic and analytical methods in synoptic dynamics. Beijing: Scientific Publishing House; 1989, pp. 114–6 [in Chinese].
[49] Kuo HL. On the formation and intensification of tropical cyclones through latent heat release by cumulus convection. J Atmos Sci 1965;22(1):40–63.
[50] Kuo HL. Further studies of the parameterization of the influence of cumulus convection on large-scale flow. J Atmos Sci 1974;31(5):1232–40.
[51] Zhang XW. The expression of the modified ***Q*** vector and its application. J Trop Meteorol 1999;15(2):162–7, [in Chinese].
[52] Carr FH, Bosart LF. A diagnostic evaluation of rainfall predictability for tropical storm Agnes, June 1972. Mon Wea Rev 1978;106(3):363–74.
[53] Dimego GJ, Bosart LF. The transformation of tropical storm Agnes into an extratropical cyclone, part II: Moisture, vorticity and kinetic energy budgets. Mon Wea Rev 1982;110(5):412–33.
[54] Ding YH, Liu YZ. Study on vapor budget of the typhoon No. 7507. Acta Ocean Sin 1986;8(3):291–301, [in Chinese].
[55] Lin Y-L, Chiao S, Wang TA, et al. Some common ingredients for heavy orographic rainfall. Wea Forecasting 2001;16(6):633–60.